

Maps of Ionospheric F2-Layer Characteristics Derived from GPS Radio Occultation Observations

Lung-Chih Tsai^{1,2,*}, Chao-Han Liu^{2,3}, Tung-Yuan Hsiao⁴, and Chia-Chia Chang³

¹Center for Space and Remote Sensing Research, National Central University, Chung-Li, Taiwan, ROC

²Graduate Institute of Space Science, National Central University, Chung-Li, Taiwan, ROC

³Institute of Astronomy and Astrophysics, Academia Sinica, Taipei, Taiwan, ROC

⁴Department of Information Technology, Hsing Wu College, Taipei, Taiwan, ROC

Received 30 January 2008, accepted 7 July 2008

ABSTRACT

The Global Positioning System (GPS) radio occultation (RO) technique has been used to receive multi-channel GPS carrier phase signals from low Earth orbiting (LEO) satellites and demonstrate active limb sounding of the Earth's ionosphere. Applying Abel inversion through compensated total electron content (TEC) values, the GPS RO observations can obtain ionospheric electron density (n_e) profiles and then scale F2-layer characteristics including $foF2$ and $hmF2$, especially, $hmF2$ that cannot be directly deduced from ionosonde observations. From the GPS/MET and FS3/COSMIC missions, we can collect on average two hundred and eighteen hundred vertical n_e profiles, respectively, within one day. The retrieved $foF2$ and $hmF2$ results have been used to produce numerical maps representing complex properties on a world-wide scale. This paper presents a physically appealing representation of $foF2$ and $hmF2$ medians based on GPS RO data. The derived numerical maps have also been examined by ground-based ionosonde data.

Key words: Ionosphere, Electron density, Mapping, Radio occultation, GPS

Citation: Tsai, L. C., C. H. Liu, T. Y. Hsiao, and C. C. Chang, 2009: Maps of ionospheric F2-layer characteristics derived from GPS radio occultation observations. *Terr. Atmos. Ocean. Sci.*, 20, 535-546, doi: 10.3319/TAO.2008.07.07.02(AA)

1. INTRODUCTION

The ionosphere is that region of the earth's atmosphere in which free ions and electrons exist in sufficient abundance to affect the properties of electromagnetic waves that are propagated within and through it. The structure of the ionosphere is highly variable. The F2 region is the strongest ionospheric region, and it is also the most variable in time and in space. For the most used empirical ionosphere model, the International Reference Ionosphere (IRI) model (Bilitza 2001), models of the F2-layer critical frequency ($foF2$) and the peak density height ($hmF2$) are expressed in terms of elementary functions of latitude, longitude and universal time, multiplied by appropriate coefficients (Rush et al. 1984; URSI 1987) that have been determined by applications of spherical harmonic analyses on the ionosonde data. These analyses are referred to as numerical mapping of $foF2$ and $hmF2$. It is based on vertical-incidence ionosonde observa-

tions from ~150 stations throughout the world and theoretically generated $foF2$ and $hmF2$ values to improve representations over ocean and other inaccessible areas. Furthermore, $hmF2$ values cannot be directly deduced from ionosonde observations and then used in corresponding numerical mapping. For an assumption of a simple ionospheric layer, in which the variation of n_e with height is parabolic with plasma frequency, the virtual height at a plasma frequency of $0.834 foF2$ in the absence of the Earth's magnetic field equals $hmF2$ and can be used to estimate $hmF2$. Other techniques for estimating $hmF2$ can be carried out by the conversion of a plasma frequency versus virtual height curve to an n_e true height profile, i.e., true height analyses, or determined by empirical equations with the transmission factor $M(3000)F2$ and a correction (M) to $M(3000)F2$, formulated in terms of the ratio $foF2/foE$ (Dudeney 1983) as used in the IRI model. We suggest that physically appealing representations of $foF2$ and $hmF2$ are possible using GPS RO data. An advantage is data compilation includ-

* Corresponding author
E-mail: lctsay@csrsr.ncu.edu.tw

ing areas over oceans and the southern hemisphere, where few ionosonde stations are positioned. The purpose of this article is to describe $foF2$ and $hmF2$ mapping using GPS RO observations and to investigate the possibility of incorporating RO data in future numerical coefficients. To map $foF2$ and $hmF2$ parameters, we first discuss the achievable accuracy of input RO data. In sections 3 and 4, spherical harmonic analysis and optimization of $foF2$ and $hmF2$ numerical coefficients are discussed. Throughout GPS/MET and FormoSat3/Constellation Observing System for Meteorology Ionosphere and Climate (FS3/COSMIC) data, the corresponding mapping results of spherical harmonic analysis are further discussed in sections 5 and 6, respectively.

2. IONOSPHERIC SOUNDING EXPERIMENTS FROM GPS/MET AND FS3/COSMIC

Probing Earth's atmosphere and ionosphere via GPS RO observations from a LEO satellite was proposed by Jet Propulsion Laboratory in 1988 but was first implemented by the University Corporation for Atmospheric Research (UCAR) (Zou et al. 1995; Ware et al. 1996; Kursinski et al. 1997; Rocken et al. 1997). UCAR launched the MicroLab-1 satellite at a nearly circular orbit of ~ 735 km altitude and $\sim 70^\circ$ inclination angle in 1995. The main objectives of this GPS-to-LEO RO mission were numerical weather prediction and long-term monitoring of the Earth's climate and thus it was termed the GPS/Meteorology (GPS/MET) program. Besides which, GPS/MET has also been able to sound the ionosphere from its orbit altitude to the Earth's surface and retrieve one-dimensional profiles of ionospheric n_e from measurements of ray-path bending angle or TEC (Hajj and Romans 1998; Hocke and Igarashi 2002a). In the GPS/MET mission, the MicroLab-1 spacecraft was equipped with a single antenna that tracked the occulted GPS satellites of setting (or rising) behind the Earth's ionosphere at an angle less than ~ 60 degrees between the occultation plane and the LEO orbital plane. A GPS receiver onboard the MicroLab-1 satellite provides up to 250 useful RO observations per day based on 24 GPS satellites. After the GPS/MET mission, further missions flown with GPS RO receivers onboard include the Danish Ørsted, the German CHAMP, the Argentinean SAC-C, the American-German GRACE, the South African SUNSAT, and the Ionosphere Occultation Experiment (IOX) onboard the PICOSAT satellite. After those, the Taiwan FS3/COSMIC satellites were successfully launched on 15 April 2006. In relation to the GPS/MET mission, the FS3/COSMIC project placed six micro-satellites into different orbits at ~ 800 km altitudes, and each micro-satellite was equipped with two high-gain occultation antennas to track both rising and setting GPS satellites. RO measurements on board FS3/COSMIC will cover the entire global atmosphere and ionosphere, providing over 2500 sounding data per day.

When receiving multi-channel GPS carrier phase signals from LEO satellites, an occultation takes place when a GPS satellite sets or rises behind the Earth's ionosphere and lower atmosphere as seen by a receiver in LEO. Each occultation therefore consists of a set of limb-viewing links with ray perigee ranging from the orbiting LEO satellite to the surface of the Earth. n_e profiles can be derived, in general, by Abel inversion through the computation of calibrated TEC values under the assumptions of locally spherical symmetry and straight-line propagation. There are several studies examining and estimating the accuracy of retrieved GPS/MET n_e profiles obtained with Abel inversions by comparing them with vertical ionosonde data (Hajj and Romans 1998; Schreiner et al. 1999; Tsai et al. 2001). All studies concluded satisfactory peak densities retrieved from RO observations with fractional root-mean-square (*rms*) differences from 10% to 20% in $foF2$. Without additional data interpretation the retrieved n_e s actually suffer from inherent horizontal averaging in Earth angle. To improve spatial resolution and accuracy Straus (1999) and Hajj et al. (2000) have presented a constrained-gradient Abel inversion method, which uses earlier simulated horizontal gradients from other ancillary data (*in-situ* plasma density, nadir-viewing extreme ultraviolet airglow, and vertical TEC maps derived from ground-based GPS receivers) and constrains the practical Abel inversion considering the horizontal asymmetry effect on n_e retrieval. Hocke and Igarashi (2002b) also proposed a two-dimensional recovery method, which can compute electron density within a meridian plane at all latitudes and from the top layer of the LEO satellite altitude to the base of the ionosphere. Meanwhile, both Hernandez-Pajares et al. (2000) and Garcia-Fernandez et al. (2003) have also developed modified Abel inversion algorithms expressing the three-dimensional retrieved n_e as the product of a vertical TEC map and a shape function in altitude that provided better statistics than the traditional Abel inversion assuming spherical symmetry. Another improved scheme was also proposed by Tsai and Tsai (2004) and Tsai et al. (2009). The effect of large-scale horizontal gradient in n_e was taken into consideration by introducing a compensation procedure for measured TEC values through several close-up RO observations. The TECs could be "compensated" by the ray integral of n_e differences between the spherical symmetry n_e and the interpolated two-dimensional n_e from a set of close-up profiles retrieved from earlier inversion. Applying the compensated TECs to the Abel inversion again and again could reduce error from the spherical symmetry assumption and approach a reliable result. Our investigation showed improved agreement with the ionosonde data when the grouped RO observation number is larger than 3. From several hundred thousand matches within the FS3/COSMIC intense observation period experiment, evaluation of the FS3/COSMIC retrieved $foF2$ s through the improved Abel inversion scheme (after two iterations) on compensated TECs is shown

in Fig. 1. Results of underestimated and overestimated $foF2$ s are obtained in high $foF2$ values (from 4.5 to 9 MHz) and low $foF2$ values (from 2 to 4 MHz), respectively, but the fractional mean and rms $foF2$ differences are significantly improved. The average rms $foF2$ differences between the ionosonde measurements and the FS3/COSMIC retrievals are improved from 1.67 to 1.07 MHz.

As described ionosonde observations cannot provide $hmF2$ directly and be used to verify retrieved GPS RO $hmF2$ values. In this paper, we have simulated path TECs by integrating the IRI-modeled n_{es} . n_e profiles can then be retrieved by our improved Abel inversion scheme through simulated TECs. Such simulation is called a “reference” GPS RO experiment in this paper. The retrieved n_e profiles can then be compared and verified by the “true” IRI-modeled ionosphere. Figure 2 illustrates a scatter plot and the corresponding least-squares fitting line for the retrieved GPS RO $hmF2$ values versus the “true” $hmF2$ values based on the IRI model. The results have a high linear correlation coefficient of 0.98 and a fitting line with a slope of 0.98 and a positive bias of 5.50 km. The corresponding average mean and rms $hmF2$ differences are -2.62 and 6.59 km, respectively, which is about the same as typical range resolution scales of ionosonde sounding.

3. SPHERICAL HARMONIC ANALYSIS OF IONOSPHERIC CHARACTERISTICS MAPPING

The construction of a particular solution of the Laplace’s partial differential equation on the surface of a sphere (assumed independent of time) is known as spherical surface harmonics. The numerical map for $foF2$ or $hmF2$ can denote a spherical harmonic function, (θ, ϕ) , in spherical coordinates of θ θ 180 and ϕ ϕ 360, and the spherical surface Laplace equation is:

$$\frac{1}{\sin \theta} \frac{\partial}{\partial \theta} \left(\sin \theta \frac{\partial \Gamma}{\partial \theta} \right) + \frac{1}{\sin^2 \theta} \frac{\partial^2 \Gamma}{\partial \phi^2} = 0 \quad (1)$$

where θ is the geographic latitude added by 90, ϕ could be the geographic longitude (in the Earth coordination) or the local time angle (in the local time system coordination) measured westward from apparent noon (i.e., 0 denotes noon, and 180 denotes midnight). The resulting real functions obtained on separation of variables and the Gram-Schmidt orthogonalization process (Davis 1989) are defined by:

$$U_{nm}(\theta, \phi) = \sqrt{\frac{2n+1}{2\pi} \frac{(n-m)!}{(n+m)!}} P_n^m(\cos \theta) \cos m\phi \quad (2)$$

and

$$V_{nm}(\theta, \phi) = \sqrt{\frac{2n+1}{2\pi} \frac{(n-m)!}{(n+m)!}} P_n^m(\cos \theta) \sin m\phi \quad (3)$$

$$(n = 0, 1, 2, \dots; m = 0, 1, 2, \dots, n),$$

where

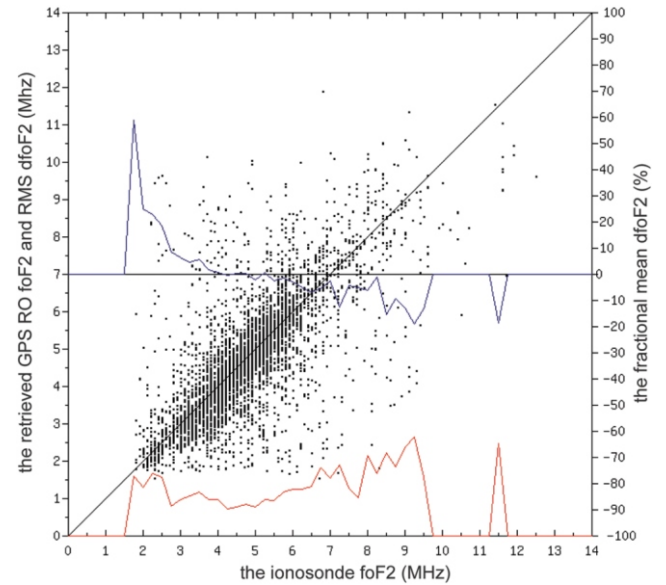


Fig. 1. A scatter plot of the FS3/COSMIC retrieved $foF2$ s versus the scaled $foF2$ from ionosonde data, their rms $foF2$ difference curve in red (refer to the left y-axis in MHz), and their fractional mean $foF2$ difference curve in blue (refer to the right y-axis in percentage) as a function of the ionosonde $foF2$.

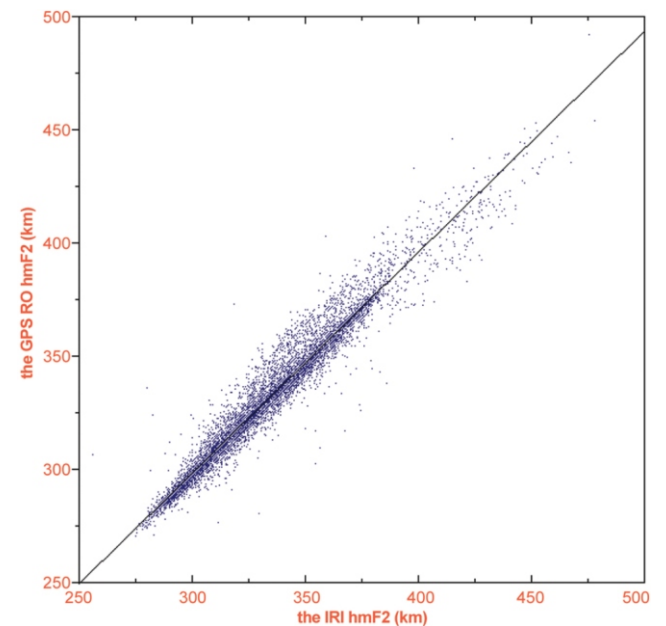


Fig. 2. A scatter plot of the retrieved GPS RO $hmF2$ s from a reference GPS RO experiment versus the true $hmF2$ s from the IRI model.

$$P_n^m(\cos \theta) = \frac{1}{2^n} \sin^m \theta \sum_{l=0}^{\lfloor \frac{n-m}{2} \rfloor} (-1)^l m! \binom{n-2l}{m} \binom{n}{l} \binom{2n-2l}{n} \cos^{n-m-2l} \theta \quad (4)$$

is the familiar associated Legendre polynomial of the first kind of degree n and order m . The above explicit expression for the associated Legendre function is extracted by the authors. The geographic variation of $foF2$ or $hmF2$ can thus be represented by a series of functions, $U_{nm}(\theta, \phi)$ and $V_{nm}(\theta, \phi)$, analogous to the Earth surface. Notice that the functions $U_{nm}(\theta, \phi)$ and $V_{nm}(\theta, \phi)$ are orthogonal and normal sets in terms of the inner product. There are exactly $2n + 1$ linearly independent spherical surface harmonics of degree n ; these functions are called tesseral spherical harmonics for $m < n$ and sectorial spherical harmonics for $m = n$. In theory, any continuous function on the surface of a sphere can be uniformly approximated there by means of these orthogonal spherical harmonics with any desired degree of accuracy. In this study, we will choose as our coordinate functions a particular set of the spherical surface harmonics $U_{nm}(\theta, \phi)$ and $V_{nm}(\theta, \phi)$ in the first three orders of $m = 0, 1$, and 2 only but an optimum degree for each order to separate noise from real longitudinal variation. The determination of the optimum order and degree numbers will be discussed in details within the next section. The spherical harmonics in the order of $m = 0, 1$, and 2 are respectively specified for terms involving the main latitudinal trend without longitudinal variation, tesseral harmonics ($m = 1$) for including first order longitudinal variation, and second order sectorial and tesseral order harmonics ($m = 2$) for including second order longitudinal variation. The optimum number of terms for $foF2$ and $hmF2$ geographic variation in each order is made by truncating high spectrum harmonics based on a least-square fitting. It is assumed that the values q_0, q_1 , and q_2 are the highest powers of $\cos\theta$ for each of the three orders, and the values k_0, k_1 , and k_2 could be specified as the term index k at the end of each order and are related to the q -values as follows:

$$\begin{aligned} k_0 &= q_0 + 1, \text{ and} \\ k_r &= k_{r-1} + 2(q_r + 1) \text{ for } r = 1, 2 \end{aligned} \quad (5)$$

A least-square representation in the form of a linear combination of $U_{nm}(\theta, \phi)$ and $V_{nm}(\theta, \phi)$ has many properties of a spherical harmonic analysis. For example, it is periodic in latitude and longitude; the first and second order sectorial and tesseral harmonics are linear combinations of the first and second order longitude variation terms which are weighted according to latitude by the functions \sin and \sin^2 , respectively. Meanwhile, the fitting of polynomials in \cos

has the effect of pulling the data symmetrically away from the equator toward the poles, and the data becomes more uniformly distributed in \cos than in θ (or the latitude). Furthermore, at high degrees the powers in \cos have much larger absolute values and thus the polynomials in \cos become more wildly fluctuating (i.e., unstable) near the poles than near the equator. In contrast, the polynomials in \cos can also minimize the maximum error and are as stable at the poles as they are at the equator. Figure 3 firstly shows an example representation of $foF2$ main latitude variation for the 13th prime GPS/MET daytime data using least-square fitting polynomials in both θ (red line) and \cos (blue line) of degree 12. It was found that the latitudinal variation could be represented in more detail by the polynomial in \cos than in θ of the same degree. Moreover, more stable representations near the poles were obtained by using the polynomial in \cos , too. More examples representing higher order longitudinal variation will be discussed in the following sections.

4. OPTIMUM SEPARATION OF NOISE

In this paper, input ionospheric data ($foF2$ and $hmF2$) are affected by noise produced from a number of sources including limitations of equipments, retrieval techniques such as the Abel inversion method, and intrinsic random fluctuations of the physical phenomena being measured. Generally, the values of noise are small compared to the main physical variations; they are assumed to be distributed independently and normally with mean zero and standard deviation σ . Thus a certain amount of smoothing is necessary for numerical mapping, but its effect must be carefully studied since we wish to represent the physical characteristic with as much detail as possible. The method employed here is based on residuals between the $foF2$ or $hmF2$ values being fitted and the fitting values from a smoothing (or filtering) process by truncating a series of spherical surface functions, $U_{nm}(\theta, \phi)$ and $V_{nm}(\theta, \phi)$, described in the previous section. A standard deviation e_K of the residuals can be defined as following:

$$E_K = \sum_{i=1}^N \left\{ y_i - \sum_{m=0}^2 \sum_{n=0}^{q_m} [A_{nm} U_{nm}(\theta_i, \phi_i) + B_{nm} V_{nm}(\theta_i, \phi_i)] \right\}^2, \quad \text{and } e_K^2 = \frac{E_K}{N - K - 1}$$

$$[K = k_2 = q_0 + 1 + 2(q_1 + 1) + 2(q_2 + 1)], \quad (6)$$

where E_K is the sum of squares of residuals at a term number of K (or k_2 defined in the last section), N is the number of $foF2$ or $hmF2$ measurements, y_i , (being also the RO observation number), and $(N - K - 1)$ is the number of degrees of freedom remaining after subtraction of one degree for each term in the series $U_{nm}(\theta, \phi)$ and $V_{nm}(\theta, \phi)$. At specified order and degree numbers for the spherical surface functions the coefficients A_{nm} and B_{nm} can be determined by the

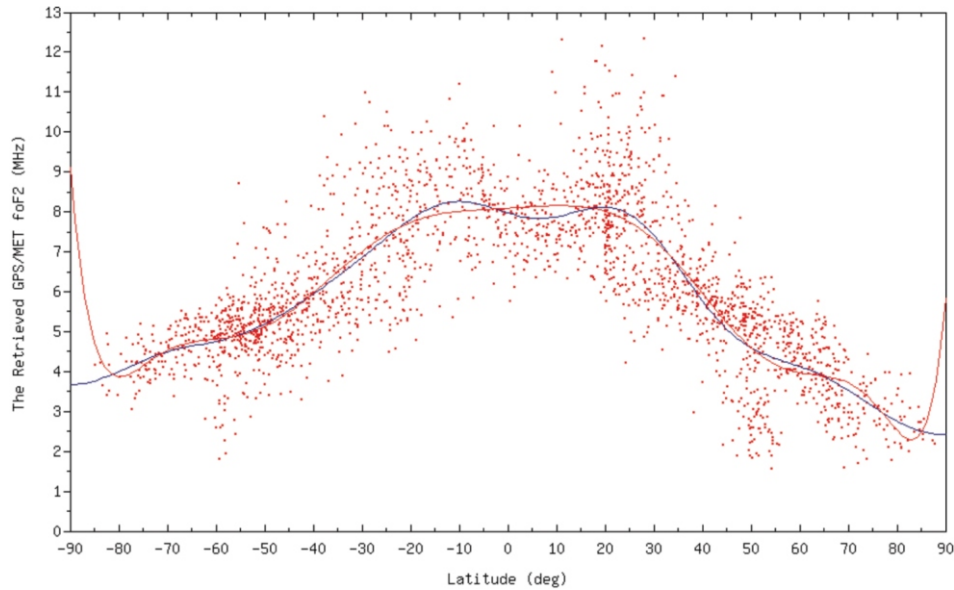


Fig. 3. An example representation of $foF2$ main latitude variation for the 13th prime GPS/MET daytime data using least-square fitting polynomials of degree 12 in both latitude (red line) and cos (blue line).

method of least squares. The residuals in Eq. (6) are modeling residuals, which are not equal to input data errors from retrieving or measurements. Residuals can approach zero as the number K of terms in the series increases. However, we know the retrieved $foF2$ s and $hmF2$ s are affected by noise; hence zero residuals are not desired. In the least squares analysis under each order, the values e_K usually decrease at first at a rate dependent upon the smoothness of (θ, ϕ) , taper off, and cease to diminish appreciably after a certain point of cutoff. Our problem is therefore to give more objects and quantitative estimation of the noise for its optimum separation from real physical variation by means of mathematical data analyses. The smoothing (filtering) in the geographic dimensions is performed by determining the best term indexes k_0, k_1 , and k_2 (or the degree indexes q_0, q_1 , and q_2) for the orthogonal series for $foF2$ and $hmF2$ mapping. The sum of coefficient squares is convergent, therefore, a necessary condition for the convergence of a series is that the general term approaches zero. It is shown (Davis 1989) that if the numerical map (θ, ϕ) has a continuous derivative of n^{th} order, an absolute amplitude C_{nm} can be defined as $(A_{nm}^2 + B_{nm}^2)^{1/2}$ and approach zero at least as fast as n^{-n} . The criterion adopted for determining the optimum cutoff is therefore to search for a tendency to level off the absolute amplitude. When C_{nm} is plotted against n in a log-log scale, the curve defined by smoothing the points on the graph will have a slope less than or equal to $-n$. It is safe to assume that the geographic variation of $foF2$ or $hmF2$ has at least a piecewise continuous first derivative. Thus the slope of its log-log relationship between the squared amplitude and the degree number should be -1 or less. To illustrate the method, each of the thirteen prime

time data of the GPS/MET mission has been divided into eight parts each of which is of a 45-degree geomagnetic longitude range and mostly has more than 400 RO observations. Spherical harmonic analysis was performed separately for each part. Figure 4 shows the average C_{nm} against the degree number n in a log-log scale at each of the first four orders (blue line for the zero-order analysis, cyan line for the first order analysis, red line for the second order analysis, and brown line for the third order analysis). It is shown that the smoothed slopes of C_{nm} for the first three order analyses (not including the third order analysis) appear to be less than -1 but larger than -2 in agreement with the theory. In the zero-order analysis the graph of C_{nm} against n shows a tendency to level off around degree 24, giving the optimum cutoff q_0 . In a similar manner we determine the optimum cutoffs to be degrees 20 and 15 for the first and second order terms q_1 and q_2 in longitude.

5. $foF2$ AND $hmF2$ MAPPING RESULTS OF THE GPS/MET MISSION

In this study, an improved Abel inversion scheme has been applied to GPS/MET RO observations and more than forty thousand ionospheric n_e profiles and corresponding $foF2$ and $hmF2$ values within 13 prime times (~ 250 days) were collected from April 1995 to February 1997. There are on average about thirty-five hundred RO observations recorded within a GPS/MET prime time (about twenty days). The beginning and ending days and the numbers of recorded RO observations for all primes are shown in the first four columns of Table 1. In the following, $foF2$ and $hmF2$ mapping functions have been developed with a total term

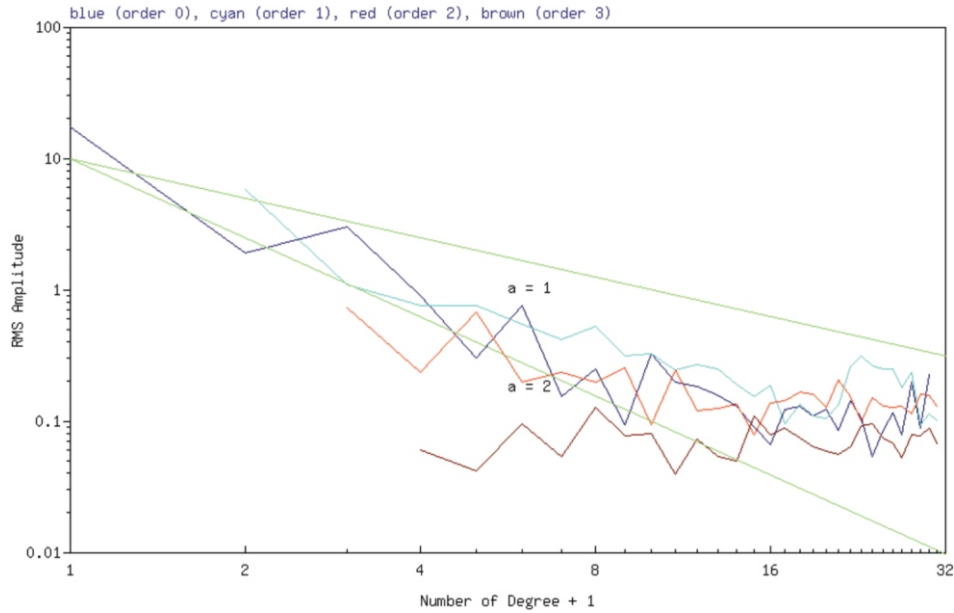


Fig. 4. Graphs of the average amplitude versus the degree number at the 0th (in blue), 1st (in cyan), 2nd (in red), and 3rd (in brown) group order. The $a = 1$ and $a = 2$ lines (in green) show the slopes of its log-log relationship to be -1 and -2, representing a piecewise continuous first and second derivative map, respectively.

Table 1. Estimates of standard deviation error for a numerical mapping $foF2$ representation from GPS/MET observations.

Prime #	1	2	3	4	5	6	7	8	9	10	11	12	13
Beginning day	95'/108	95'/170	95'/223	95'/283	95'/328	96'/022	96'/076	96'/128	96'/186	96'/237	96'/293	96'/350	97'/033
Ending day	95'/130	95'/192	95'/242	95'/305	95'/349	96'/042	96'/097	96'/148	96'/207	96'/258	96'/312	97'/005	97'/054
Number of occultation	1275	4158	3265	4160	3008	3296	3923	3180	3812	3552	2777	4274	4766
A/S status	OFF	OFF	ON	OFF	ON	OFF							
Frequencies of Kp indices (> 3)	72	25	23	49	24	19	38	6	4	40	33	6	33
Standard deviation (MHz) of $foF2$ fitting	1.02	0.77	0.84	1.09	0.92	0.89	0.98	0.77	0.72	0.88	1.11	0.97	0.90

number, K , of 99 ($q_0 = 24$, $q_1 = 20$, and $q_2 = 15$). These functions (λ , θ) therefore can represent the continuous time variations of an ionospheric F2-layer critical frequency characteristic on a world-wide basis and can be used to compute its value at any desired location and instant in time. Such functions are referred to as numerical maps. In this study, mostly more than four hundred $foF2$ and $hmF2$ values have been used to determine a series of spherical surface functions to produce a numerical map for each prime time and every 45-degree geomagnetic longitude range. As described the geographic variation of retrieved $foF2$ and $hmF2$ values can thus be represented by a series of spherical harmonic functions analogous to the Earth surface in the lati-

tude and local time system coordination. Example results of mixed latitudinal and longitudinal $foF2$ and $hmF2$ variation are illustrated by the two-dimensional images of Figs. 5 and 6, respectively, using the 13th prime time GPS/MET data at the geomagnetic longitude ranges of 90 ~ 135 . The solid points from Figs. 5 and 6 denote the line-of-viewing tangent point locations at the F2 peak of RO observations. The local time angle 0 denotes noon and 180 denotes midnight. As pointed out in section 2, the Microlab-1 spacecraft of the GPS/MET mission was equipped with a single antenna that tracked the occulted GPS satellites in view of setting (or rising for a few percentages) behind the Earth's ionosphere at an angle less than ~60 degrees of the occultation plane out of

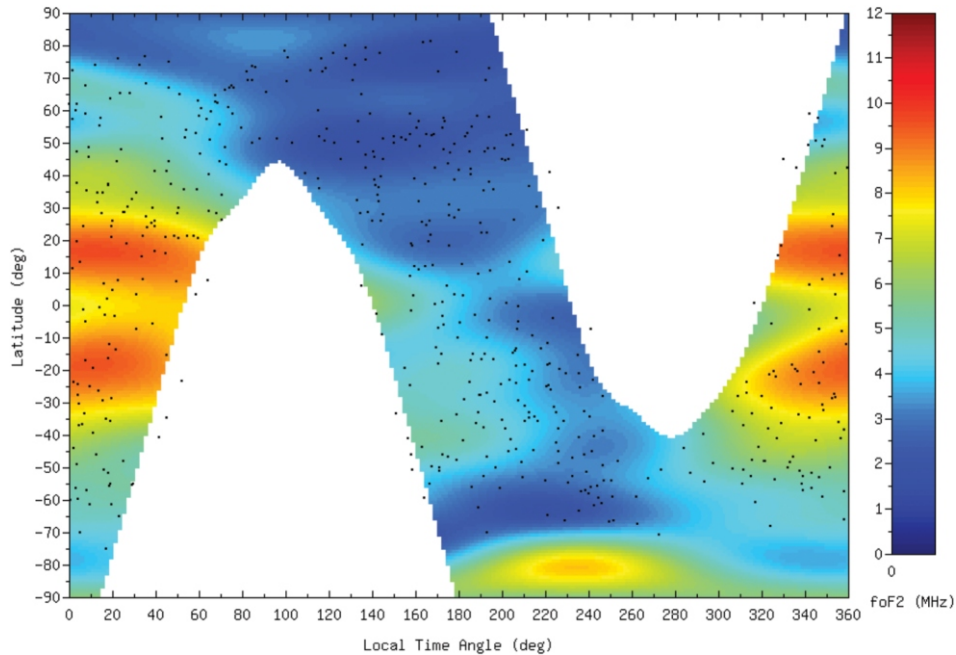


Fig. 5. Mixed latitude and second order longitude trend $foF2$ mapping using the GPS/MET 13th prime time data at 90 ~ 135 geomagnetic longitudes.

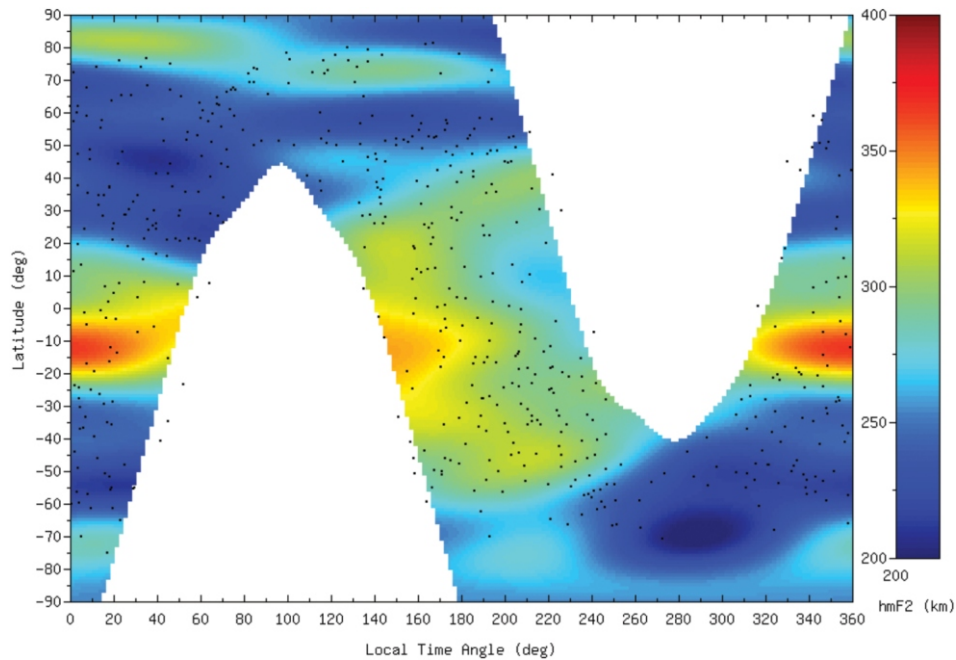


Fig. 6. Mixed latitude and second order longitude trend $hmF2$ mapping using the GPS/MET 13th prime time data at 90 ~ 135 geomagnetic longitudes.

the LEO orbital plane. Since the MicroLab-1 satellite was located at a nearly circular orbit of ~ 735 km altitude and $\sim 70^\circ$ inclination angle to receive GPS signals, the GPS RO observations are irregularly distributed onto part of the Earth surface which covers most of the latitudes between the poles but only ~ 30 longitudinal degrees from both sides of

the LEO orbit. Therefore, to obtain an “effective” representation of the geographic $foF2$ and $hmF2$ variation, we just consider the colored areas where GPS RO observations were available as shown from Figs. 5 and 6. In the regions of low-latitude and daytime (the local time angle < 100 or > 300) as shown in Fig. 5, the $foF2$ s are clearly higher than

the values in high-latitude and/or recorded at nighttime. Furthermore, for both images of Figs. 5 and 6, we note that, in the dayside (the local time angle $< 100^\circ$ or $> 300^\circ$) equatorial and low-latitude region, features of the equatorial anomaly were observed during the local time period from 8 am to 6 pm.

To further evaluate the goodness of the fits of spherical surface function coefficients, the rows from 2nd to 7th in Table 1 list the beginning and ending days, the numbers of recorded RO observations, the GPS A/S status of each prime time, the analyzed standard deviation of $foF2$ mapping, and the analyzed standard deviation of $hmF2$ mapping. As discussed, the noise (or error) of representation of F2-layer characteristic will be studied in terms of residuals obtained from subtracting numerical map values from corresponding RO data. The residuals might be due to random deviations caused by noise inherent in ionospheric data and small systematic variations that have not been represented. As shown in Table 1, the resulting standard deviation of residuals from the mapping analysis of RO $foF2$ values remains fairly stable at less than 0.86 MHz within the GPS/MET mission and has a mean value of 0.74 MHz. The standard deviation values of different prime times are not related to the numbers of RO observations and nor GPS A/S status. It can be seen that the $foF2$ values determined by the numerical mapping yield smaller residuals, for examples of: 0.66, 0.68, 0.64, and 0.62 MHz for the 2nd, 3rd, 8th, and 9th prime data analyses, respectively, in the middle of the years than at the beginning (or end) of the years. Meanwhile, Fig. 7 shows the standard deviation values (refer to the right y-axis) in solid points and the profile of monthly frequencies (refer to the

left y-axis) of geomagnetic Kp index values larger than 2. Kp indices are based on the range of variation within a 3-hour period of the day observed from about a dozen selected magnetic observations and serve a practical function as the basis of geophysical activity on a scale from 0 (for 'very quiet') to 9 (for 'very disturbed'). We note there are comparative low frequencies of Kp larger than 2 at the 2nd, 3rd, 8th, and 9th prime times of GPS/MET when the numerical mapping of $foF2$ also yields smaller residuals.

6. $foF2$ AND $hmF2$ MAPPING RESULTS BASED ON THE FS3/COSMIC DATA

In the FS3/COSMIC mission, all six spacecraft (FM1 to FM6) were integrated and launched together into a parking orbit of 515 km altitude; whereupon each spacecraft was separated and then transferred from the parking orbits to their final orbits at ~ 800 km. Figure 8 shows daily orbit ascending angles of the six FS3/COSMIC spacecraft. Similar orbit ascending angles for all six spacecraft were presented at the beginning of FS3/COSMIC mission; FM5 was transferred firstly onto the targeted orbit, and then FM2, FM6, FM4, FM3, and FM1 finally. The final spacecraft orbits are separated into 30 degrees and the daily RO measurements on board FS3/COSMIC are distributed uniformly onto the entire atmosphere and/or ionosphere after 2007. A comprehensive view of the numbers of RO measurements on board FS3/COSMIC and successfully retrieved n_e profiles from each spacecraft is shown in Fig. 9. Since 28 July 2006, raw excess phase data and the retrieved n_e profiles are available from the Taiwan Analysis Center for COSMIC

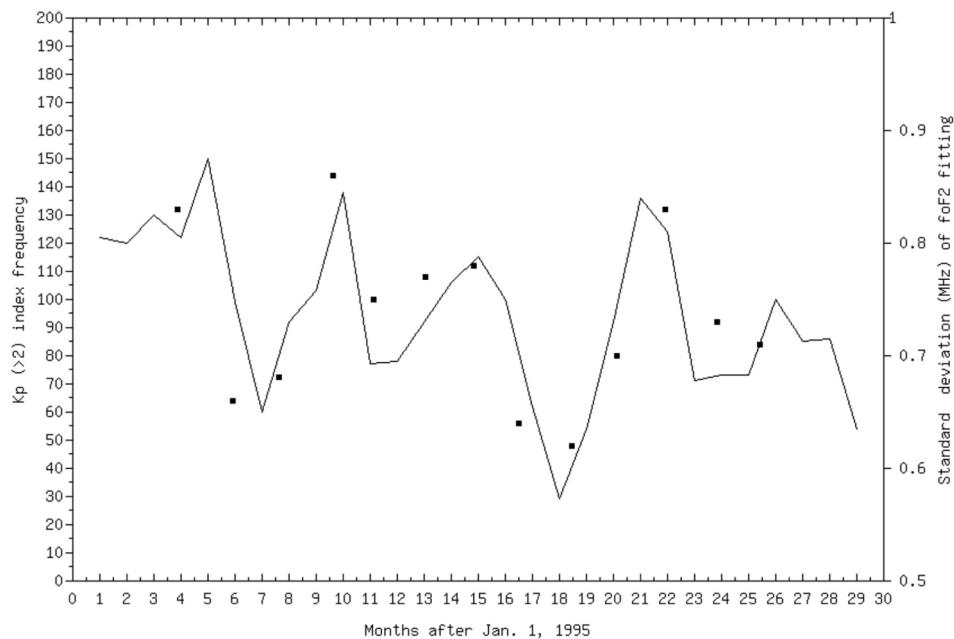


Fig. 7. The comparison between the standard deviation of $foF2$ mapping and the monthly frequencies of geomagnetic Kp index values larger than 2.

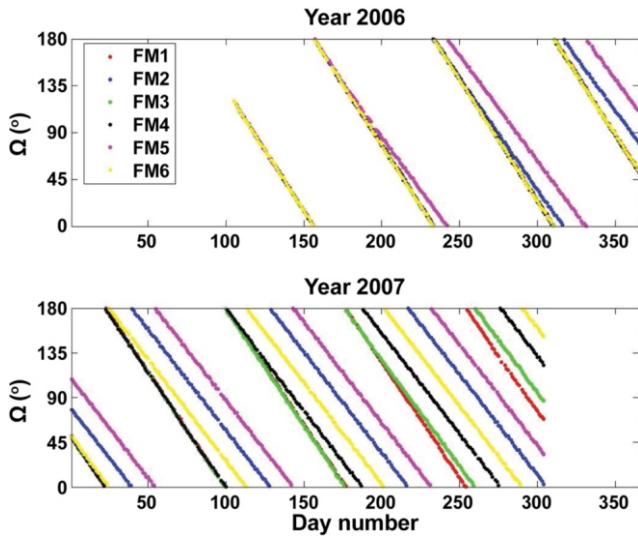


Fig. 8. Daily orbit ascending angles of the six FS3/COSMIC spacecraft.

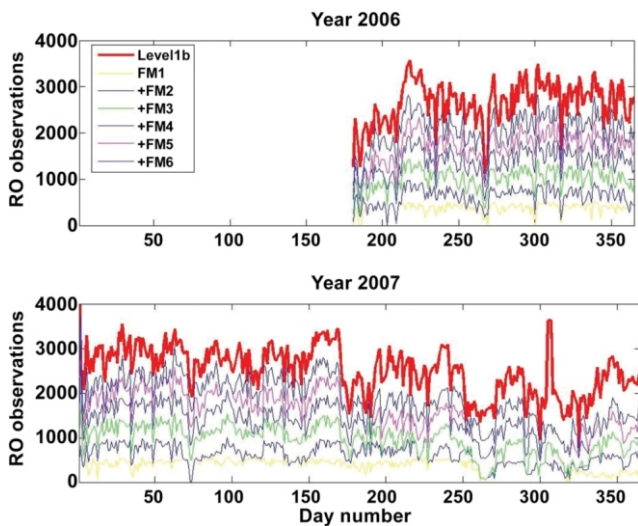


Fig. 9. A comprehensive view of GPS RO measurements (in red) on board FS3/COSMIC and the accumulated numbers of n_e profiles successfully retrieved and summed up from FM1, FM2, FM3, FM4, FM5, and then FM6.

(TACC, <http://tacc.cwb.gov.tw/en/>) and the COSMIC Data Analysis and Archive Center (CDACC, <http://www.cosmic.ucar.edu/cdacc/>). Generally FS3/COSMIC can perform over 2500 RO measurements per day, and more than 70% of the RO measurements can be successfully retrieved into n_e profiles. For the remaining RO measurements the atmospheric excess phase calibration failed and the n_e profiles could not be obtained. The failed measurements were usually caused by locking onto GPS carrier signals either starting too late or ending too early.

As described, there are on the average about eighteen hundred n_e profiles and corresponding $foF2$ and $hmF2$ re-

trieved per day within the FS3/COSMIC mission. In the following, we have applied spherical harmonics analyses on monthly $foF2$ and $hmF2$ values at geographic coordinates and within every local time (LT) hour. Example results of $foF2$ and $hmF2$ numerical maps are illustrated by the two-dimensional images in Figs. 10 and 11, respectively, using the FS3/COSMIC data in August, 2007. From Figs. 10 and 11, the solid points denote the line-of-viewing tangent point locations at the F2 peak of RO observations, and three curves in black present positions with magnetic dip latitudes of $+30^\circ$, 0° , and -30° from the top down. The top-left, top-right, bottom-left, and bottom-right images in Fig. 10 (Fig. 11) represent the 2007 August $foF2$ ($hmF2$) numerical map at: 0200, 0800, 1400, and 2000 LT, respectively. From Fig. 10 the highest-latitude area in the south is in continual darkness and has lower n_e than the highest-latitude area at the north that is in continual daylight because its summer. Features of the diurnal ionosphere variations are obtained and illustrated as follows. The $foF2$ s are greater by day than by night; $foF2$ increases promptly after sunrise and continues to increase for a few hours after noon and then decreases. There is a general tendency for $hmF2$ to fall at dawn and then rise during the afternoon or evening. In low latitudes and at the equator, $hmF2$ reaches a high level by about 1400 LT and then falls such that by late at night it is about 100 km lower than in the afternoon, and the F2 layer is much thicker near the equator than elsewhere particularly in the daytime. Furthermore, we note that, in equatorial and low-latitude regions, features of the equatorial anomaly are observed in the daytime, and two $foF2$ crests lie along the $+30^\circ$ and -30° magnetic dip latitudes. The features are developed after sunrise and become strongest at about 1400 LT. It is well known that equatorial anomaly results are something of the equatorial fountain feature and are caused by an eastward electric field at the magnetic equator creating a steady upward $\mathbf{E} \times \mathbf{B} / B^2$ plasma drift. The drift raises plasmas from the equator across magnetic field lines to higher altitudes. After losing momentum, the electrons slide down, assisted by gravity, along the field lines to either side of the equator to form two crests. This is called the fountain effect (Hanson and Moffett 1966). One important factor is that ionization changes due to $\mathbf{E} \times \mathbf{B}$ drift are particularly matched to magnetic dip latitude and north-south asymmetry effects; these are incorporated and shown in Figs. 10 and 11, too. Theoretically, in the absence of neutral winds, the upward $\mathbf{E} \times \mathbf{B}$ drift produces almost identical effects at conjugate points; however, neutral winds can cause conjugate-hemisphere differences by modulating the fountain and moving ionospheric electrons at the conjugate hemispheres to different altitudes. Complete mapping images and modeling coefficients based on FS3/COSMIC data can be found from “<http://140.115.111.228/>”, hosted by the Center for Space and Remote Sensing Research, National Central University, and are organized in exactly the same form as in section 4.

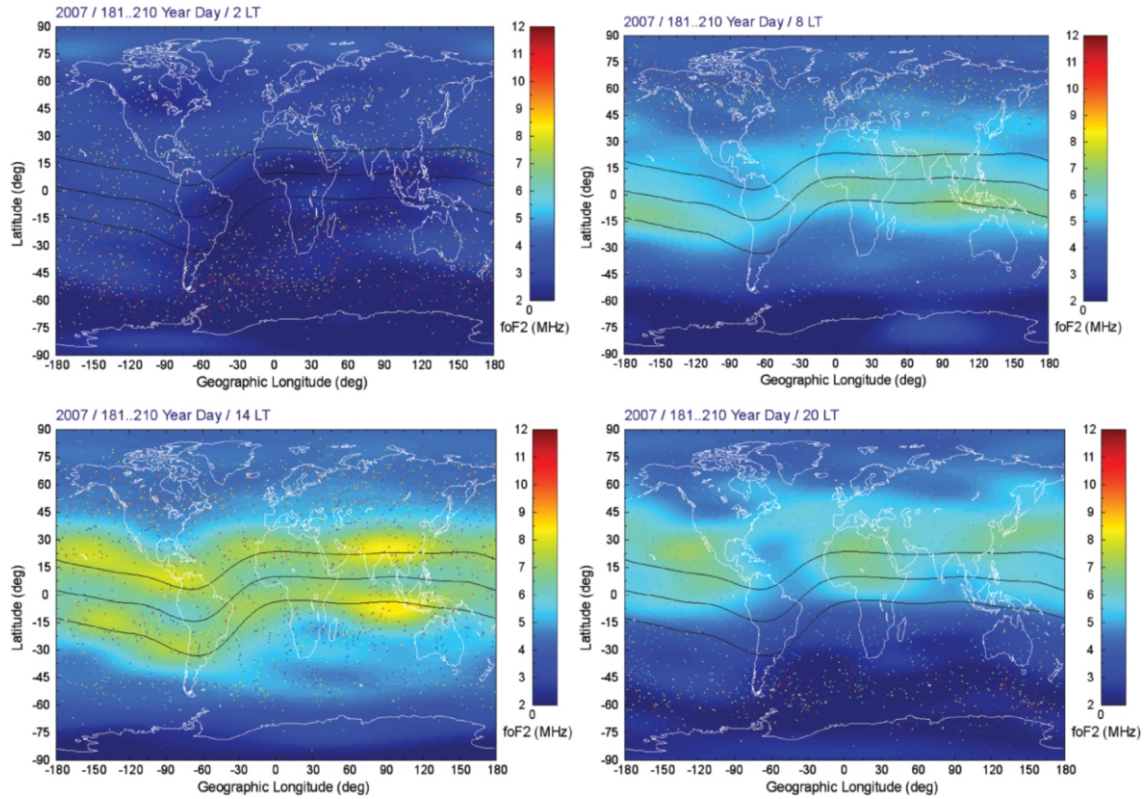


Fig. 10. The 2007 August $foF2$ numerical maps at 0200, 0800, 1400, and 2000 LT are assigned to the top-left, top-right, bottom-left, and bottom-right images, respectively. The solid points denote the line-of-viewing tangent point locations at the F2 peak of RO observations, and three curves in black present positions with magnetic dip latitudes of +30 , 0 , and -30 from the top down.

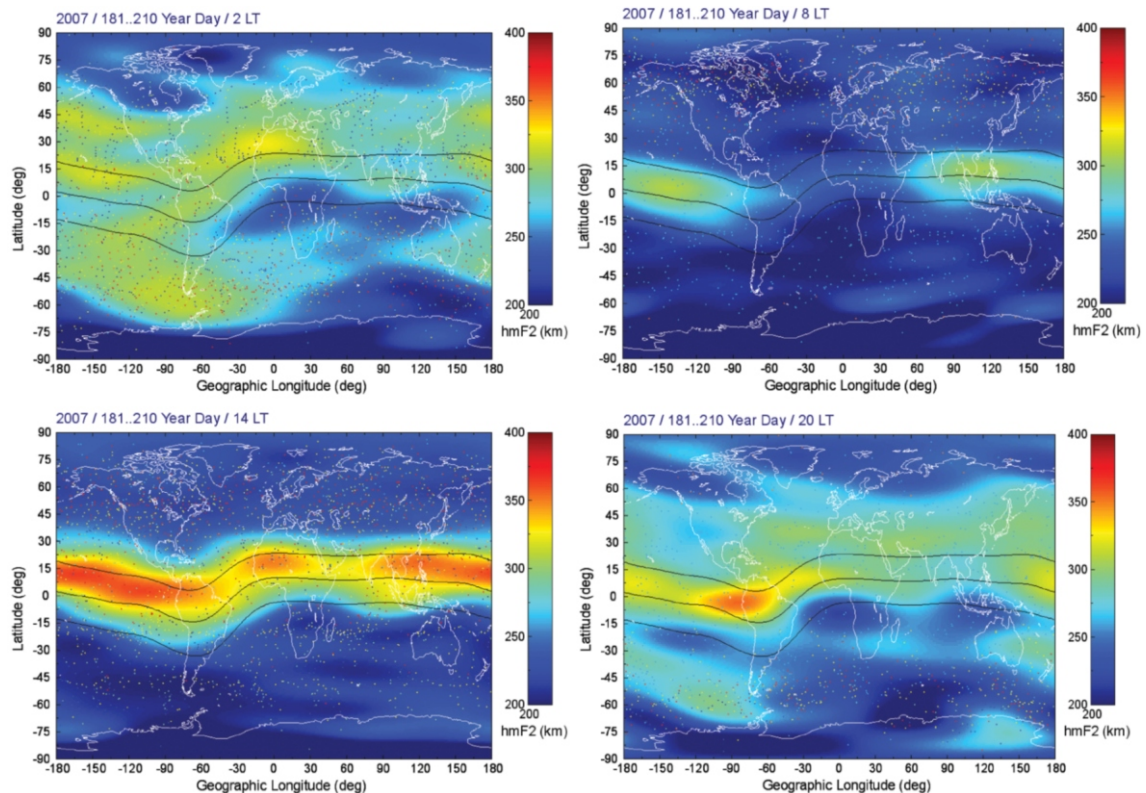


Fig. 11. The 2007 August $hmF2$ numerical maps at 0200, 0800, 1400, and 2000 LT are assigned to the top-left, top-right, bottom-left, and bottom-right images, respectively.

7. CONCLUSIONS

We conclude here that a physically appealing representation of $foF2$ and $hmF2$ is possible using GPS RO data. An advantage is data compilation that includes oceans and the southern hemisphere, where fewer ionosonde stations are positioned. Mapping analysis can be performed in different coordinate systems. We choose as our coordinate functions a particular set of the spherical surface harmonics $U_{nm}(\theta, \phi)$ and $V_{nm}(\theta, \phi)$ in the first three orders of $m = 0, 1$, and 2 only, but allow an optimum degree for each order to separate noise from real longitudinal variation. For the optimum separation of noise, we adopt a criterion whereby optimum cutoff is to search for a tendency to level off the absolute amplitude. Making use of the distributions of RO observations, we have computed the standard deviations of the $foF2$ medians, too. In periods of low geomagnetic activity within the GPS/MET mission, $foF2$ values determined by numerical mapping have smaller residuals in the middle than at the beginning (or end) of years. Furthermore, the new GPS RO mission of FS3/COSMIC could provide twelve times power of magnification for RO observations to determine more dense regions and the global distribution of $foF2$ and $hmF2$ in numerical mapping. Calculations of average noise in $foF2$ and $hmF2$ medians made over a period of several years is found to be closely correlated with geophysical activity. These investigations give very valuable information on large regions of the world, especially over seas where no dense networks for ionospheric observations exist.

Acknowledgements This work has been supported by Projects 96-NSPO(B)-SP-FA07-02-L and NSC96-2111-M008-008-012.

REFERENCES

- Bilitza, D., 2001: International Reference Ionosphere 2000. *Radio Sci.*, **36**, 261-275, doi: 10.1029/2000RS002432. [\[Link\]](#)
- Davis, H. F., 1989: Fourier Series and Orthogonal Functions, Dover Publications, Inc., New York.
- Dudeney, J. R., 1983: The accuracy of simple methods for determining the height of the maximum electron concentration of the F2-layer from scaled ionospheric characteristics. *J. Atmos. Terr. Phys.*, **45**, 629-640, doi: 10.1016/S0021-9169(83)80080-4. [\[Link\]](#)
- Garcia-Fernandez, M., M. Hernandez-Pajares, M. Juan, and J. Sanz, 2003: Improvement of ionospheric electron density estimation with GPSMET occultations using Abel inversion and VTEC information. *J. Geophys. Res.*, **108**, 1338-1344, doi: 10.1029/2003JA009952. [\[Link\]](#)
- Hajj, G. A. and L. J. Romans, 1998: Ionospheric electron density profiles obtained with the Global Positioning System: Results from the GPS/MET experiment. *Radio Sci.*, **33**, 175-190, doi: 10.1029/97RS03183. [\[Link\]](#)
- Hajj, G. A., L. C. Lee, X. Pi, L. J. Romans, W. S. Schreiner, P. R. Straus, and C. Wang, 2000: COSMIC GPS ionospheric sensing and space weather. *Terr. Atmos. Ocean. Sci.*, **11**, 235-272.
- Hanson, W. B. and R. J. Moffett, 1966: Ionization transport effects in the equatorial F region. *J. Geophys. Res.*, **71**, 5559-5572.
- Hernández-Pajares, M., J. M. Juan, and J. Sanz, 2000: Improving the Abel inversion by adding ground GPS data to LEO radio occultations in ionospheric sounding. *Geophys. Res. Lett.*, **27**, 2743-2746, doi: 10.1029/2000GL000032. [\[Link\]](#)
- Hocke, K. and K. Igarashi, 2002a: Structure of the Earth's lower ionosphere observed by GPS/MET radio occultation. *J. Geophys. Res.*, **107**, 1057, doi: 10.1029/2001JA900158. [\[Link\]](#)
- Hocke, K. and K. Igarashi, 2002b: Electron density in the F region derived from GPS/MET radio occultation data and comparison with IRI. *Earth Planets Space*, **54**, 947-954.
- Kursinski, E. R., G. A. Hajj, J. T. Schofield, R. P. Linfield, and K. R. Hardy, 1997: Observing Earth's atmosphere with radio occultation measurements using the Global Positioning System. *J. Geophys. Res.*, **102**, 23429-23465, doi: 10.1029/97JD01569. [\[Link\]](#)
- Rocken, C., R. Anthes, M. Exner, D. Hunt, S. Sokolovskiy, R. Ware, M. Gorbunov, W. Schreiner, D. Feng, B. Herman, Y.-H. Kuo, and X. Zou, 1997: Analysis and validation of GPS/MET data in the neutral atmosphere. *J. Geophys. Res.*, **102**, 29849-29866, doi: 10.1029/97JD02400. [\[Link\]](#)
- Rush, C. M., M. PoKempner, D. N. Anderson, J. Perry, F. G. Stewart, and R. Reasoner, 1984: Maps of f_oF_2 derived from observations and theoretical data. *Radio Sci.*, **19**, 1083-1097, doi: 10.1029/RS019i004p01083. [\[Link\]](#)
- Schreiner, W. S., S. V. Sokolovskiy, C. Rocken, and D. C. Hunt, 1999: Analysis and validation of GPS/MET radio occultation data in the ionosphere. *Radio Sci.*, **34**, 949-966, doi: 10.1029/1999RS900034. [\[Link\]](#)
- Straus, P. R., 1999: Correcting GPS occultation measurements for ionospheric horizontal gradients. Proc. of Iono. Effect Symp., Alexandria, VA, June.
- Tsai, L. C. and W. H. Tsai, 2004: Improvement of GPS/MET ionospheric profiling and validation with Chung-Li ionosonde measurements and the IRI. *Terr. Atmos. Ocean. Sci.*, **15**, 589-607.
- Tsai, L. C., W. H. Tsai, W. S. Schreiner, F. T. Berkey, and J. Y. Liu, 2001: Comparisons of GPS/MET retrieved ionospheric electron density and ground based ionosonde data. *Earth Planets Space*, **53**, 193-205.
- Tsai, L. C., C. H. Liu, and T. Y. Hsiao, 2009: Profiling of ionospheric electron density based on FormoSat-3/COSMIC data: Results from the intense observation period experiment. *Terr. Atmos. Ocean. Sci.*, **20**, 181-191, doi: 10.3319/TAO.2007.12.19.01(F3C). [\[Link\]](#)
- URSI, 1987: Report of URSI Working Group G. 5 on mapping of characteristics at the peak of the F2 layer, Information Bulletin No. 243, Brussels, 93-96.
- Ware, R., M. Exner, D. Feng, M. Gorbunov, K. Hardy, B.

Herman, Y. Kuo, T. Meehan, W. Melbourne, C. Rocken, W. Schreiner, S. Sokolovskiy, F. Solheim, X. Zou, R. Anthes, S. Businger, and K. Trenberth, 1996: GPS sounding of the atmosphere from low Earth orbit: Preliminary results. *Bull. Amer. Meteor. Soc.*, **77**, 19-40, doi: 10.1175/

1520-0477(1996)077<0019:GSOTAF>2.0.CO;2. [[Link](#)]
Zou, X., Y.-H. Kuo, and Y.-R. Guo, 1995: Assimilation of atmospheric radio refractivity using a nonhydrostatic adjoint model. *Mon. Wea. Rev.*, **123**, 2229-2249, doi: 10.1175/1520-0493(1995)123<2229:AOARRU>2.0.CO;2. [[Link](#)]